Comparative Analysis Over Tribology Characterization of TiAlN and TiAlSiN PVD Coating On Plasma Nitride Alloy 20

R. Ganapathy Srinivasan (krgsrini@gmail.com)
Vel Tech Multi Tech Dr Rangarajan Dr Sakunthala Engineering College

S Palani
VEL TECH MULTITECH

C Rajaravi
Park College of Engineering and Technology Coimbatore

S Karthik
Vel Tech Rangarajan Dr.Sagunthala R&D Institute of Science and Technology

Research Article

Keywords: Alloy 20, Plasma Nitriding, TiAlN / TiAlSiN PVD coating, Corrosion, Wear, Mechanical properties

Posted Date: January 11th, 2022

DOI: https://doi.org/10.21203/rs.3.rs-1232392/v1

Abstract

The nickel-iron-chromium (alloy 20) is enriching by hybrid surface treatment through plasma nitride (PN) and physical vapor deposition (PVD) process. The plasma nitriding process takes 12 hours at 500°C. Potentiodynamic testing is used to characterize the corrosion performance of the treated material, followed by morphological analysis of the exposed surface; XRD, EDX, SEM, hardness, and tensile testing are used to investigate appropriate coating properties. Plasma nitride and hybrid PVD nickel-iron-chromium alloys exhibit perlite (γ + α ′) phases and martensite (γ + α) phases, respectively. The martensite microstructure ensures superior tensile strength and hardness. The pin-on-disc tribometer test proposes to analyze friction and hard-faced behavior in the dry sliding position. The inclusion of Si improves the adherent oxide film, resulting in a low wear rate in TiAlSiN alloy 20. Due to the presence of the passive film, TiAlSiN alloy 20 exposes the most passive region to attain better corrosion resistance.

1. Introduction

Nickel (Ni) - Iron (Fe) –Chromium (Cr) alloy (Alloy 20) is highly desirable for use in aggressive chemical environments with excellent mechanical properties due to its composite properties. The presence of chromium (Cr) provides an inert film of Cr_2O_3 on the alloy surface, giving it significant passivation [1–4]. However, with lower surface hardness (210 HV), the resulting mechanical wear resistance (abrasion and adhesive) is limited. Therefore, surface protection with hardening treatment such as PVD coating and plasma nitriding attracted more attention. [5–7]. Based on the literature review [8 & 9] In the plasma nitriding process at low temperature (500°C), PN prefers Ni-Fe-Cr-based FCC austenite structure alloy. When subjected to low temperatures, the alloy behaves similarly to austenitic steel. If the temperature of the Ni-based alloy rises above 500°C, it forms a dark etched CrN precipitate on the surface. Plasma nitriding also leads to the hardening of the Ni-rich alloy, which enriches the surface properties of various nitride components (Ni_xN, Fe_xN, Cr_xN) [10–12]. The atomic-scale structure of the nitrogen-modified surface zone has been reported to be trapped in octahedral aspects by nitrogen chromium, which has developed a short-distance distribution order. Both long-order Fe4N and short-order Cr-N are stoichiometric nitrides with compound phases in the surface zone. [13–15].

A surface coating of anti-wear for pre-nitriding material enhanced nitriding durability. Physical vapour deposition (PVD) coating or chemical vapour deposition (CVD) coating can be used to deposit these coatings. They have excellent mechanical qualities, particularly good adhesion and abrasion resistance of the material layer on the surface. The nitriding substrate was protected from local damage and oxidation by the coating, while the nitride diffusion layer shows a reduction in the steady-state of varying hardness, with an intermediate layer installed between the hard coating and the soft substrate.

This prevents cracking and coating removal from the substrate. PVD coating creates a rough surface layer, which leads to removal and exclusive wear when using high normal loads. This mechanism of hybrid PVD treatment is shown in Figure 1. TiAlN surface coating can improve enhanced tribology properties by oxidation since the formation of Al_2O_3 stable phases. However, microstructure changes

from the cubic (B1) to the hexagonal (B4) phase reduce the antioxidant and mechanical properties at higher temperature environments. TiAlN has offered good wear resistance, but it also improves the wear resistance of diverse components with a greater friction coefficient [16-18. Most researchers have studied the antioxidant, mechanical properties and structure of TiAlSiN coatings using various deposition process techniques. Veprek et.al [19] tested the TiAlSiN form with a vacuum arc evaporation coating process and observed exceptional thermal stability and mechanical properties. According to TiAlSiN [20], Si plays a very important role in asset resolution, establishing 2% of Si with significant thermal stability and maximum hardness (54 GPa). PN and PVD methods are manufactured with low process temperature coating layers with low harmful substrate mechanical properties. Due to the low temperature process PN can form a shallow diffusion layer and a thin composite layer. It has a 200 - 300% better service life [21] when using the hybrid dual surface treatment on materials. Plasma nitriding stimulates the intermediate layer and increases the adhesion of the PVD coating to the substrate [22].

This current experiment was conducted to produce substantial hybrid treatment material with plasma nitriding and TiAlN / TiAlSiN PVD coating alloy 20 materials. The study aims to achieve the best wear and corrosion resistant material with the appropriate surface treatment method. This study also analyzed the impact of microstructure on the concentration of tribology properties. The wear and wear characteristics of the materials have been evaluated by various standards such as Pin-on-disc, Pin-on-drum, Pin-on-flat and reciprocal ball-on-flat [23].

2. Experimental

2.1 Test Material

The subtract material is Alloy 20, which has the following composition (in weight percent): 38 Ni, 29.85 Fe, 21 Cr, 4 Cu, 3 Mo, 1 Nb, 1 Si, 0.07 C, 2 Mn, 0.045 b, 0.035 S. A 350 mm X 350 mm square plate with a thickness of 2 mm was used to make the test specimens. Table 1 shows the preparation of three types of samples.

Table 1
Description of Hardening processed specimens

Specimens	Hardening Process
PREPN	Plasma nitriding subjected on Alloy 20
PREPN / TiAlN POPVD	Alloy 20 was plasma nitrided first, and then TiAlN PVD coating has applied.
PREPN / TiAlSiN POPVD	Alloy 20 was plasma nitrided first, and then TiAlSiN PVD coating has applied.

2.2 Pre Plasma Nitriding and Post PVD Treatments

Dry air blasting removed dust and moisture from the material surface. The PREPN process was carried out at 500˚C material for 12 hrs in a vacuum chamber. A combination of 75% nitrogen and 25% hydrogen was used to maintain in the vacuum chamber. The PREPN process was then commercially deposited TiAlN / TiAlSiN coating using PVD processes. The PVD process was carried at 450˚ C, 2 x 10-3 Pa vacuum pressure Ar: N_2 gas mixture 19: 4. The γ ray non-destructive was used for surface defects of hardened materials. Electron scattering X-ray (EDAX) analysis, scanning/transmission Electron microscopy (SEM / TEM) used to study the morphology and metallurgy.

The macro/microstructure study was carried out on a hard surface measuring 10 mm x 10 mm x 2 mm. The surface of the study material was diamond polished using various emery sheets. Sheet grid sizes are 200,400,600,800, and 1200. Refresh the specimen with distilled water to achieve look like mirror surface. Finally, the surface polished by NaCl (70%) + HCl (30%) solution. The hardness was examined by the Vickers hardness method with a load of 500 kg and a 10-second interval at a regular distance of 0.25 mm. The hardness was examined by the Vickers hardness method under a weight of 500 kg at 10-second intervals at a regular distance of 0.25 mm.

3. Results And Discussion

3.1 XRD Analysis

X-ray diffractogram analysis of alloy 20 material is shown in the figure 2 (a). A previous investigation [26] revealed that the alloy 20 γ austenite phases peaked with the face cubic centre. The diffractogram for the plasma nitriding alloy 20 are significantly changed from the basic specimens. It has provided two predicted FCC phases. The iron nitrides γ'Fe_4N (200) / γ'Ni_4N (221) and expanded austenite γN (111) are observed as the higher order of nitrogen atoms. This shows that the alloy 20 austenite lattice expanded to γN during the nitriding process. Notably, the γFe_4N (200) lattice expansion reaction is larger than the γN (111) reflection. It has been proposed that the expansion γN of the heterogeneous lattice. This expansion suggested that the nitrogen and plastic decomposition retained in γN may be limited. The presence of a slip line on the nitriding surface demonstrates this effect. This effect induced micro pressure on the nitriding layers [24 & 25]. Other than limited $Fe_{2-3}N$ (021) and iron oxides (Fe_XO_X) peaks (400), the dual morphology of alloy 20 in γ'Fe4N / γNi4N is observed. Figure 2 (b) shows X-ray diffractogram of the phase components of PREPN / TiAlN POPVD treatment alloy 20. The Ti (103) / TiAl (113) peaks are observed at the specified angular range of 20˚ to 45˚ due to the POPVD coating. These peaks are known as titanium aluminium nitride TiAlN (206) and titanium nitride TiN (221), Ti_2N (222), Ti_2N (220), as well as another high-order peak Fe (110). These peaks form a thick composite layer. No antioxidant peak was shown from this specimen. Oxidative peaks are dissolved during TiAlN POPVD evaporation processes in the PREPN process.

$$\gamma'Fe_4N/\ \gamma'Ni_4N \text{ or } \varepsilon Fe_{2-3}N \rightarrow \alpha Fe + \{N\}_{released}$$

X-ray diffractogram analysis of PREPN / TiAlSiN POPVD hardened alloy 20 is presented in figure 2 (c). The Si_3N (106) and AlN (200) are referred peaks to as TiAlN POPVD peaks. Hybrid hardening alloy 20 revealed excellent peaks as a presence of the composite layers. Reduce plastic deformation by the release and scattering and evaporation of nitrogen atoms by the POPVD compressive stresses [27 & 28]. TiAlSiN POPVD propagated the microstructure of amorphous Si_3N crystals and solid solution compounds (TiN, AlN, and SiN).The presence of Si achieves a uniform distribution with the grain refining and amorphous silicon nitride percolation phenomenon of crystals. High-quality TiN films may be composite with the formation of the Si and Al. POPVD hardened alloy 20 material appears to be golden by presence of δTiN.

3.2 Microstructure characterization of PREPN alloy 20

Figure 3 shows the surface morphology of hardening alloy 20. The SEM examination demonstrates that the difference between the treated sample surface and significant development in surface morphology. Figure 3 (a) shows that the PREPN applied at 500°C for 12 hours during diffusion was effectively transferred to γ + α' which was converting the austenite phase to pearlite [26]. Even when low temperatures are used, the phase and boundaries where transmission may be the cause of the time duration. It is believed that pearlite contributes to improved hardness. Dual-phase and twin boundaries can be induced in the microstructure. Twin boundaries expose by shear stress and plastic deformation during the plasma nitriding process. Nitrogen becomes trapped and acts as a barrier to nitrogen diffusion when it reaches the twin boundaries. The SEM analysis reveals that sharp grain boundaries as ion sputtering selective etching and expanded austenite an isotropic swelling. Figure 3 (a) shows a slip step owing to surface deformation by pearlite layer expansion. SEM analysis reveals composite layer and the diffusion layer. The diffusion layers exist as a result of N and nitrogen diffusivity. The compound layers attribute γ'Fe4N, εFe2-3N, and composite nitrides. The SEM analysis reveals that the concentration of nitrogen decreases from the surface. Because of mobility and temperature, the major alloy components Cr – Ni have no discernible redistribution throughout the compound layer. The oxide layers can be formed during diffusion by post–oxidation with air and/or pre – oxidation vacuum. PREPN alloy 20 has a grey colour due to the precipitation of nitrides and oxides on the surface. Figure 3 (b) shows the presence of micro cleavage cracks, voids, pinholes, and pores caused by oxygen passing through the grain boundaries and pores, as well as strain and deformation during cooling. The EDX analysis of plasma nitride alloy 20 is shown in Figure 3 (c). Nitrogen is evenly distributed across the treated surface. Sudha et al [29] discovered that the peak composition was the thermodynamic unstable compound formation in the nitride layers (Ni, Fe, Cr, and Mn_XN).

3.3 Microstructure characterization of PREPN / POPVD alloy 20

The cross-section SEM images in figure 4 (a) illustrate the low composite layer thickness of 12μ m TiAlN POPVD alloy 20, while comparing with 13 μm TiAlSiN POPVD alloy 20 in figure 4 (b). Rich composite layer formation can occur with Si presentation refining grain sizes. Hybrid treatment specimens scatter

particles during POPVD, filling pores and voids to form a smooth and dense TiAlN / TiAlSiN form. TiAlSiN POPVD SEM depicts a low-density dense image. Because of the low concentration of nitrogen and iron on the surface; Nitrogen and iron peaks were not found in the XRD analysis.

Figure 4 (c) depicts the PREPN / POPVD microstructure. The POPVD process triggers the application of 450°C in PREPN alloy 20 for microstructure change. The austenite and perlite (γ + α) phases promote the martensite (γ' + ε) phases. PREPN / TiAlN POPVD alloy 20 does not reveal any evidence of pinholes or voids in the surface texture. POPVD was used to deposit TiAlN under the specified conditions. Pedro Henrique Teshima Shioga et al [30] concluded process conditions contribute to developing ε and γ the composite layers and improve the hardness of the surface. The diffusion of titanium and iron particles during coating caused this smooth deposition. Although the deposition discussed in the wear analysis is not difficult, the spread also improves adhesion. The microstructure of the treated alloy can be established by forming the FCC (Ti, Al) N phase obtained by converting Al into the cubic titanium nitride phase. [31 & 32]. As a result, smooth surface forms. Figure 4 (d) depicts the formation of microstructures primarily composed of Si, where the lattice expands at the column boundaries, N mobility and displacement decrease. The TiAlSiN film showed significantly improved hardness, which may be due to the crystalline refinement due to the correlating of Si in harmony with the Hall-Betch relationship [33]. However, based on the Hall-Pitch effect, it is expected that Al integration will increase rigidity. Also, Nguyen Dang Nam et al [34] noted When added TiAlSiN surface coating revealed amorphous Si_3N_4 nanostructures with including solid –solution (Ti, Si, Al) N crystals. The significant grain distribution along with Si_3N_4 penetration was exposed. That is why an enhanced coating harness was achieved.

3.4 Corrosion Analysis of hardening alloy 20

Figure 5 shows that the results of the potentiodynamic cycle Polarization test of the hybrid surface treated alloy 20. At the potentiodynamic polarity, the test can easily assess the corrosion of the sample by using Ecorr and Icorr values. Table 2 mention potentiodynamic corrosion values. The high polarization resistance (Rp) is similar to low corrosion current density (Icorr) has excellent general corrosion resistance. The Icorr of PN /TiAlSiN is observed as 1.031 mA/cm^2 which is better than PN / TiAlN and PREPN 1.544mA/cm^2 and 1.728 mA/cm^2 respectively.

Table 2
Potentiodynamic electrochemical parameters

Samples	Ecorr (mV)	icorr (mA/cm2)	Vcorr (mm/year)
PREPN	-469.54	1.728	20.442
PN / TiAlN	-486.93	1.544	17.895
PN /TiAlSiN	-503.18	1.031	16.185

The PREPN TiAlSiN Alloy 20 has a higher corrosion resistance than other specimens because of its robust passivating layer and compressive residual stresses. Similarly, Figure 5 and Table 2 show that PREPN exhibited lower passivation than hybrid-treated specimens. Since all specimens have a hysteresis

loop, they all represent the possibility of corrosion reduction. The polar curves of the specimen revealed the passive layer breakdown capacity and corrosion current density. The polarization curves of the shot peening specimen show that the passive layer decreases as the current density increases. The potential voltage is proportional to the significant parameter and the rate of corrosion. Figure 5 shows that material decomposition occurs at a maximum rate in the better active and passive regions, which indicates the dissolution of the oxidation layer. This type of transition is not present in the coated specimen polarization curve. This could be due to the presence of an active ion diffusion film passing through the inter column. It should be noted that the rest point of TiAlSiN alloy 20 (c) is improved over PREPN alloy 20. (a).

Microstructure reinforcement and compressive residual stress caused by shot peening can have an impact on these effects. The compressive residual stresses and grain reinforcement due to plastic decomposition may be affected by increased corrosion resistance [26]. Micro pits were found on the surface of the TiAlN / TiAlSiN samples, as shown in Figure 6 (b). The martensite phases of the TiAlN/TiAlSiN samples regulated elite corrosion and confirmed the presence of micro pits. The corrosion surface of the TiAlN / TiAlSiN sample is depicted in Figure 6 (c). The addition of silicon with TiAlN affected grain growth, which resulted in better surface corrosion. There were small pits on the TiAlN / TiAlSiN treated surface and there was limited evidence for excessive corrosion damage.

3.5 Wear Analysis of hardening alloy 20

Wear rate was analyzed by mass loss data and SEM analysis as a function of the normal loads (2KN, 4KN, and 6 KN) used during the flexible wear test conducted at 15-minute intervals. The PREPN was reported as significant losses. The illustration demonstrates that the clearly varying mass loss was logical with loads. Under low normal loads (2 KN and 4 KN), PREPN / TiAlN POPVD alloy 20 showed minimal weight loss; however, there was a significant loss at 6 KN. PREPN / TiAlSiN POPVD Alloy 20 exhibits minimal loss despite excessive normal load conditions. This is approximately 35% and 15% compared to PREPN and PREPN / TiAlN POPVD Alloy 20. The POPVD treatment alloy offers excellent wear resistance due to the adhesion properties already mentioned in the PREPN / POPVD microstructure analysis. From these results, PREPN and PREPN / POPVD coating established the largest and smallest wear ratio degree, respectively. SEM analysis of wear tracks is shown in Figure 7.

Figure 7 (a) shows the wear analysis of the PREPN alloy 20. It reveals a rough surface with some pits, holes and grooves leading to adhesive wear. Figure 7 (b) was very smooth on PREPN / TiAlN POPVD Alloy 20 with minimal pits and micro holes, cracking lines. The density of the traces was relatively low compared to PREPN alloy 20. This ensured moderately low wear due to the composite layer and surface hardness. Figure 7 (c) None of the groove lines found on PREPN / TiAlSiN POPVD Alloy 20 show only micro pits and holes. Results PREPN / TiAlSiN POPVD Alloy 20 wear appears to be relatively minimal. This could be due to the thick composite layer's high surface hardness and impressive adhesive properties. Subakanya Kansaiyapham et al [35] discovered that the TiAlSiN coating has better dry wear resistance and a maximum longer sliding distance than the TiCrAlSiN and TiN coatings.

3.6 Mechanical Properties' analysis of PREPN and PREPN / POPVD alloy 20

Figure 8 shows the evolution of hardness for PREPN, PREPN / TiAlN POPVD, PREPN / TiAlSiN 20 materials. Base alloy 20 substract hardness 218 HV improved to 238 HV by PREPN Alloy 20. The PREPN was upgraded due to the austenite expanded by Perlite (γ + α ') phase change and thermo strain processing. Retained oxygen may affect hardness. PREPN / TiAlN POPVD alloy promotes hardness up to 275 HV with phase transformations of martensite (γ + α). Not only might microstructure alterations help to promotion, as could rich composite layers on the surface. The presence of Si in PREPN / TiAlSiN POPVD enabled higher hardness to 283 HV due to improved grain structures.

The tensile strength of the treated alloy 20 material is shown in Figure 10. PREPN alloy 20 has tensile strengths ranging from 620 MPa to 648 MPa. The presence of compressive stress produced by the PREPN process resulted in improved tensile properties. During tensile load, micro split cracks and pinholes propagate the cracks. The hybrid treatment aids in the improvement of tensile properties. Because of its perlite microstructure and higher hardness, PREPN / TiAlN POPVD alloy 20 has increased tensile strength to 646 MPa. The compound layer and perlite constitute low ductility phases, which improve the material's tensile strength and rigidity. Tensile strength of up to 685 MPa is promoted by PREPN / TiAlSiN POPVD. This specimen had a rich composite layer with Si presence and less evidence of surface pinholes cracking. In comparison to other models, there were few failures. The martensite phase is better ductile than the perlite phase, which has a higher tensile strength.

4. Conclusion

Investigation of the microstructure and tribology characteristics of PREPN and TiAlN / TiAlSiN POPVD in alloy 20 materials follows

- According to the experimental results, the surface-treated alloy 20 outperforms PREPN / TiAlSiN POPVD, PREPN / TiAlN POPVD, and PREPN alloy 20.
- The Microstructure analysis reveals that too (γ + α') Pearlite and to (γ + α) Martensite Phases on PREPN and PREPN / POPVD alloy 20 respectively. The phases have been occurring by thermo and thermo-chemical process care of above hardening process
- The PREPN / TiAlSiN alloy 20 exposes exclusive wear rate and corrosion resistance as 35% and 30% higher than the PREPN alloy 20.
- Due to its hardness of 283 HV and tensile strength of 685 MPa, high adhesion, and rich composite layer, PREPN / TiAlSiN Alloy 20 develops superior properties compared to the other two specimens. Furthermore, the presence of Si improves grain boundaries in (γ + α) martensite phases.

References

1. M. Razavian, S. Fatemi, A.T. Najafabadi, Extraction of highly pure nickel hydroxide from spent NiO/Al2O3 catalyst: Statistical study on leaching by sulfuric acid lixiviant and selective precipitation. J. Env.Che Eng **8**, 2 103660 (2020)
2. A.K. Mishra, N. Ebrahimi, D.W. Shoesmith, *and P. E. Manning., Materials Selection for Use in Hydrochloric Acid.In CORROSION 2016* (OnePetro, 2016)
3. M. Morcali, L.T. Hakan, Khajavi, Serdar Aktas, and David Bruce Dreisinger, Oxidative dissolution of nickel matte in dilute sulfuric acid solutions,Hydro, 2019,185,257-265
4. Z. Shi, Y. Yu, Y. Wang, D. Zhang, L. Dai, M. Wang, Effect of nickel content on the processing and microstructure evolution of Co–Cr–Mo–Ni alloys. Mat. Sci.and Eng,A,2019,759,195-202
5. M. Maja, O.E. Edith, B.A. Falodun, S.R. Obadele, Oke, and Peter Apata Olubambi., Nanoindentation studies on TiN nanoceramic reinforced Ti–6Al–4V matrix composite. Cer. Int, 2018,44, 4 ,4419-4425
6. A. Sowińska, Elżbieta Czarnowska, Michał Tarnowski, Justyna Witkowska, and Tadeusz Wierzchoń., Structure and hemocompatibility of nanocrystalline titanium nitride produced under glow-discharge conditions. App Surf. Sci **436**, 382–390 (2018)
7. Z. Zhang, X. Li, H. Dong, Response of a molybdenum alloy to plasma nitriding. International J. of Ref.Met and Hard Mat, 2018,72 388-395
8. D. Manova, S. Mändl, H. Neumann, B. Rauschenbach, Analysis of in situ XRD measurements for low energy ion beam nitriding of austenitic stainless steel. Sur and Coat Tech **256**, 64–72 (2014)
9. E. Zdravecká, J. Slota, P. Solfronk, Michaela, Kolnerová, Evaluation of the effect of different plasma-nitriding parameters on the properties of low-alloy steel. J of Mat Eng and Perf **26**(7), 3588–3596 (2017)
10. J. Wang, Y. Lin, J.Y.D. Zen, Q. Zhang, R. Huang, Hongyuan, Fan, Influence of time on the microstructure of AISI 321 austenitic stainless steel in salt bath nitriding. Surf and C Tech **206**, 15 3399–3404 (2012)
11. M. Fonović, A. Leineweber, O. Robach, E.A. Jägle, E.J. Mittemeijer, The nature and origin of double expanded austenite in Ni-based Ni-Ti alloys developing upon low temperature gaseous nitriding. Meta and Mat Trans A, 2015,46, 9,4115-4131
12. C. Sudha, R. Anand, V. Thomas Paul, S. Saroja, M. Vijayalakshmi, Nitriding kinetics of Inconel 600.Sur and Coat Tech **226**, 92–99 (2013)
13. D.L. Williamson, O. Ozturk, R. Wei, P.J. Wilbur, Metastable phase formation and enhanced diffusion in fcc alloys under high dose, high flux nitrogen implantation at high and low ion energies,Sur and Coat Tech, 1994,65,1-3, 15–23
14. J. Oddershede, T.L. Christiansen, K. Ståhl, A.J. Marcel, Somers, Extended X-ray absorption fine structure investigation of nitrogen stabilized expanded austenite. Scr Mat **62**(5), 290–293 (2010)
15. T. Bell, Current status of supersaturated surface engineered S-phase materials. In Key Eng Mat **373**, 289–295 (2008)

16. D.H. Yu, C.Y. Wang, X.L. Cheng, F.L. Zhang,,Microstructure and properties of TiAlSiN coatings prepared by hybrid PVD technology. T Sol Fil **517**, 4950–4955 (2009)
17. Z.L. Wu, Y.G. Li, B. Wua, M.K. Lei, Effect of microstructure on mechanical and tribological properties of TiAlSiN nanocomposite coatings deposited by modulated pulsed power magnetron sputtering. T Sol Fil **503**, 197–205 (2015)
18. N. He, H. Li, L. Ji, X. Liu, H. Zhou, J. Chen, High temperature tribological propertiesof TiAlSiN coatings produced by hybrid PVD technology, Tribol. Int.2016, 98,133–143
19. S. Veprek, H.-D. Männling, M. Jilek, P. Holubar, Avoiding the high-temperature decomposition and softening of (Al1– xTix) N coatings by the formation of stable superhard nc-(Al1– xTix) N/a-Si3N4 nanocomposite. Mat Sci and Eng A **366**, 1,202–205 (2004)
20. S. Carvalho, L. Rebouta, A. Cavaleiro, L.A. Rocha, J. Gomes, and E. Alves. Microstructure and mechanical properties of nanocomposite (Ti, Si, Al) N coatings. T Sol Fil **398**, 391–396 (2001)
21. B. Navinšek, P. Panjan, I. Urankar, P. Cvahte, F. Gorenjak, Improvement of hot-working processes with PVD coatings and duplex treatment. Sur and Coat Tech **142**, 1148–1154 (2001)
22. E. Damerchi, A. Abdollah-zadeh, R. Poursalehi, M. Salari, Mehr, Effects of functionally graded TiN layer and deposition temperature on the structure and surface properties of TiCN coating deposited on plasma nitrided H13 steel by PACVD method. J of Al and Com **772**, 612–624 (2019)
23. S. Khanchaiyaphum, C. Saikaew, A. Wisitsoraat, S. Surinphong, Wear behaviours of filtered cathodic arc deposited TiN, TiAlSiN and TiCrAlSiN coatings on AISI 316 stainless steel fishing net-weaving machine components under dry soft-sliding against nylon fibres. Wear **390**, 146–154 (2017)
24. K. Mukahiwa, F. Scenini, M. Grace Burke, N. Platts, D.R. Tice, J.W. Stairmand, Corrosion fatigue and microstructural characterisation of Type 316 austenitic stainless steels tested in PWR primary water. Cor Sci **131**, 57–70 (2018)
25. X. Xu, Z. Yu, L. Cui, Microstructure and properties of plasma nitrided layers on Ni-based superalloy Ni-20Cr, Mat Char,2019, 155,109798
26. R. Srinivasan, R. Ganapathy, S. Selvabharathi, Palani, R. Karuppasamy, Influence of high-velocity oxygen fuel spraying and plasma nitriding on microstructure properties of iron-nickel-chromium alloy using hybrid surface heat treatment.Mat Res Exp, 2019, 6, 8,086584
27. M. Dong, Y. Zhu, C. Wang, L. Shan, J. Li, Structure and tribocorrosion properties of duplex treatment coatings of TiSiCN/nitride on Ti6Al4V alloy. Cer Int **45**(9), 12461–12468 (2019)
28. A.F. Rousseau, J.G. Partridge, E.L.H. Mayes, J.T. Toton, M. Kracica, D.G. McCulloch, E.D. Doyle, Microstructural and tribological characterisation of a nitriding/TiAlN PVD coating duplex treatment applied to M2 High Speed Steel tools, Sur and coat tech,2015, 272,403–408
29. C. Sudha, R. Anand, V. Thomas Paul, S. Saroja, M. Vijayalakshmi, Nitriding kinetics of Inconel 600, Sur and Coat Tech **226**, 92–99 (2013)
30. P.H. Shioga, C. Teshima, G. Binder, Hammes, Aloisio Nelmo Klein, and Jose Daniel Biasoli de Mello,Effects of different plasma nitrided layers on the tribological performance of DLC coatings. Mat Res **19**, 1180–1188 (2016)

31. V. Godinho, T.C. Rojas, S. Trasobares, F.J. Ferrer, Marie-Paule Delplancke-Ogletree, and Asuncion Fernández, Microstructural and chemical characterization of nanostructured TiAlSiN coatings with nanoscale resolution. Mic and Mic **18**(3), 568–581 (2012)
32. Y.M. Liu, C.L. Jiang, Z.L. Pei, H. Lei, J. Gong, C. Sun, Microstructure and properties of AlB2-type WB2 thin films deposited by direct-current magnetron sputtering., Surf and C Tech,2014,245,108-116
33. G. Kim, B.S. Seok, S.Y. Kim, Lee, and Jun Hee Hahn., Effect of Si content on the properties of TiAl–Si–N films deposited by closed field unbalanced magnetron sputtering with vertical magnetron sources, Thin Sol Fil 506,128–132
34. N. Nam, M. Dang, Vaka, N. Tran, Hung, Corrosion behavior of TiN, TiAlN, TiAlSiN-coated 316L stainless steel in simulated proton exchange membrane fuel cell environment. J of Pow Sou **268**, 240–245 (2014)
35. S. Khanchaiyaphum, C. Saikaew, A. Wisitsoraat, S. Surinphong, Wear behaviours of filtered cathodic arc deposited TiN, TiAlSiN and TiCrAlSiN coatings on AISI 316 stainless steel fishing net-weaving machine components under dry soft-sliding against nylon fibres. Wear **390**, 146–154 (2017)

Figures

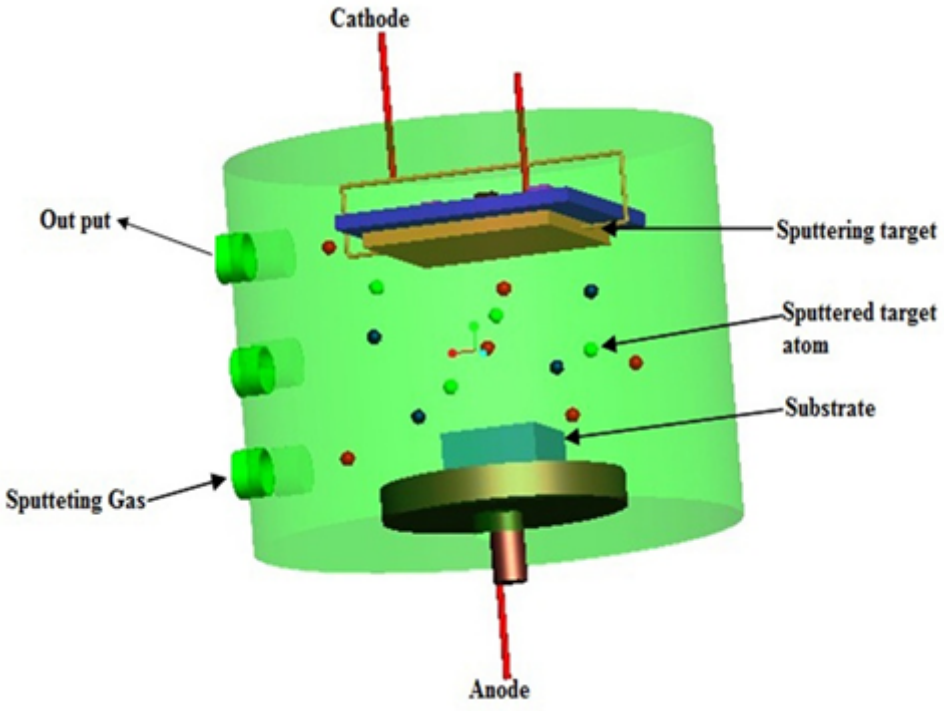

Figure 1

The PVD Process of Hybrid Treatment

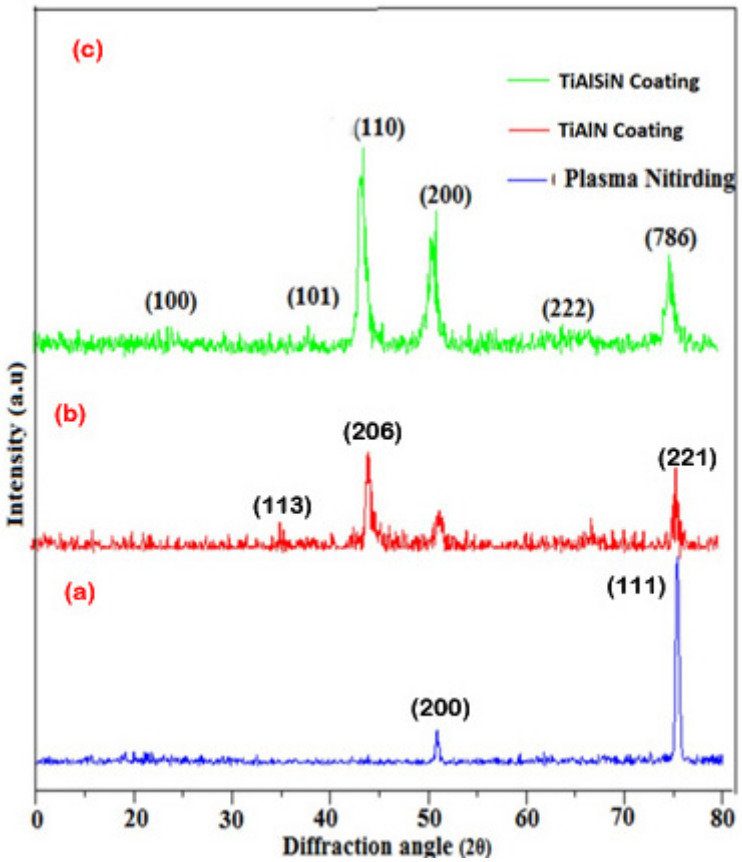

Figure 2

XRD analysis of (a) PREPN alloy 20, (b) TiAlN POPVD alloy 20 and (c) TiAlSiN POPVD

Figure 3

(a) and (b) Microstructure analysis of PREPN alloy 20 (c) EDX analysis of PREPN alloy20

Figure 4

(a) Compound layer thickness of TiAlN PREPN / POPVD (b) Compound layer thickness of TiAlSiN PREPN / POPVD (c) Microstructure analysis of TiAlN PREPN / POPVD (d) Microstructure analysis of TiAlSiN PREPN / POPVD

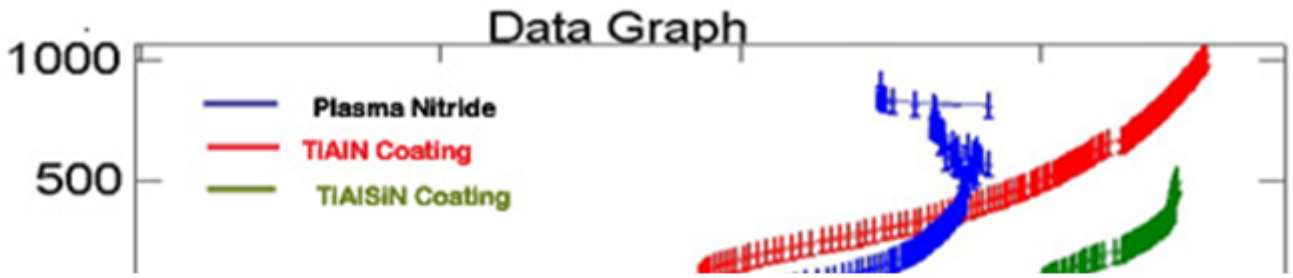

Figure 5

Potentiodynamic curves of PREPN and TiAlSiN/TiAlN POPVD alloy 20

Figure 6

Corrosion morphology of (a) PREPN alloy 20, (b) TiAlN POPVD alloy 20 and (c) TiAlSiN POPVD

Figure 7

SEM analysis of (a) PREPN alloy 20, (b) TiAlN POPVD alloy 20 and (c) TiAlSiN POPVD

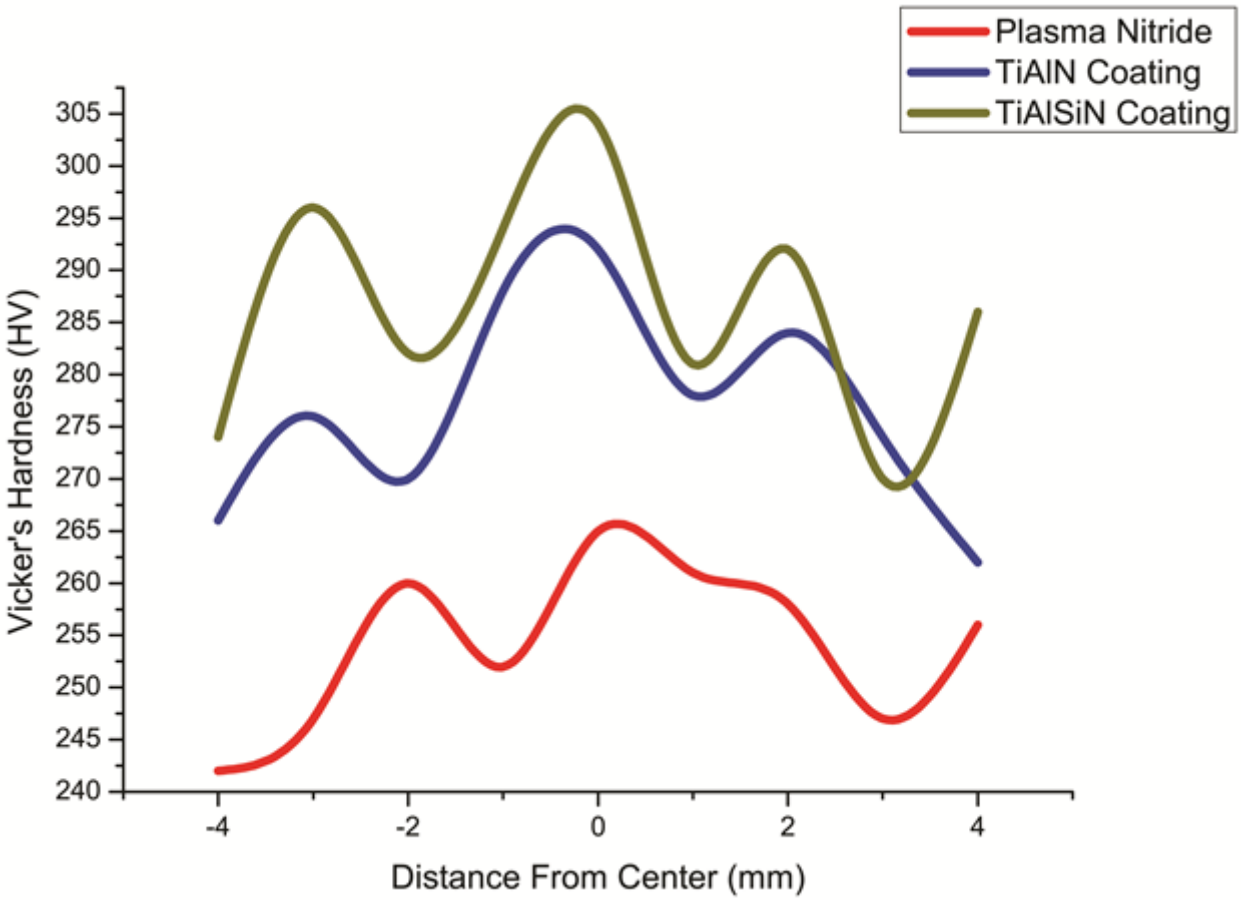

Figure 8

Hardness analysis of Treated alloy 20

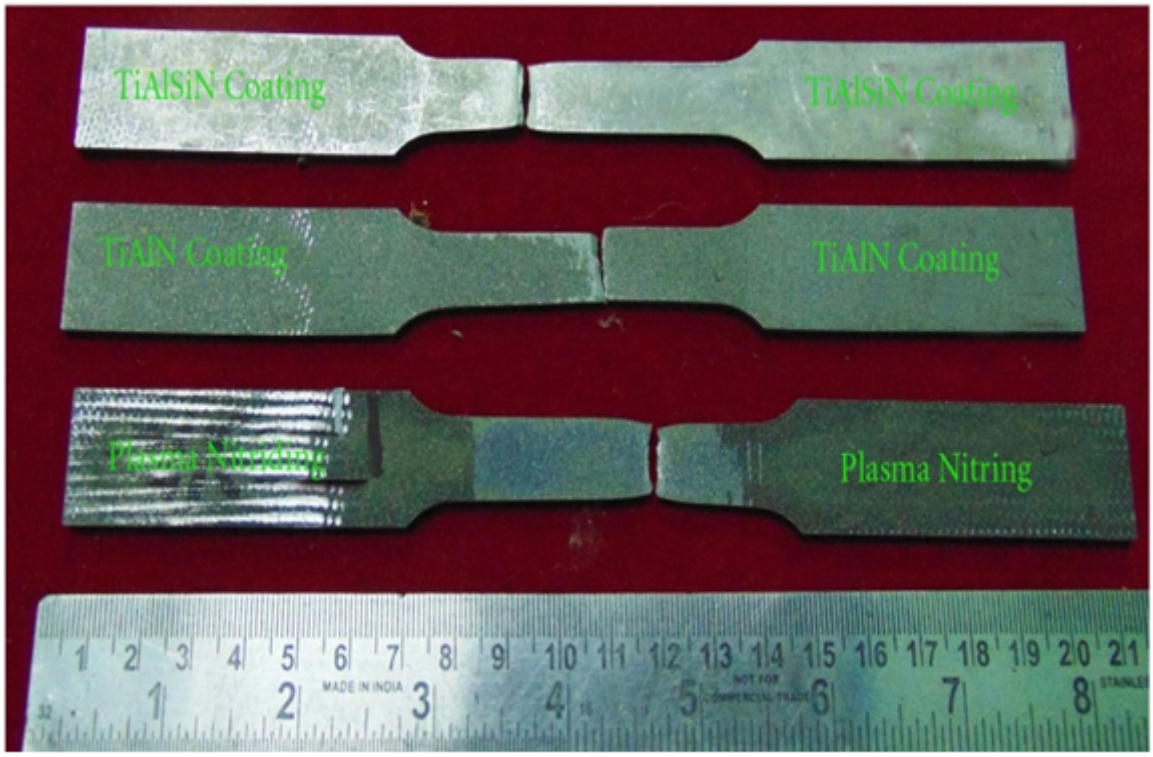

Figure 9

Tensile specimen of Treated material

Figure 10

Tensile analysis of Treated alloy 20